Nanowormlike Li$_2$FeSiO$_4$−C Composites as Lithium-Ion Battery Cathodes with Superior High-Rate Capability

Xiaozhen Wu,[†] Xuemin Wang,[‡] and Youxiang Zhang*,[†,‡]

[†]College of Chemistry and Molecular Sciences, Wuhan University, Wuhan 430072, P. R. China
[‡]State Key Laboratory of Inorganic Synthesis and Preparative Chemistry, College of Chemistry, Jilin University, Changchun 130012, P.R. China

ABSTRACT: Nanoworm-like Li$_2$FeSiO$_4$−C composites are synthesized using triblock copolymer Pluronic P123 (poly-(ethylene oxide)-*b*-poly(propylene oxide)-*b*-poly(ethylene oxide), EO$_{20}$PO$_{70}$EO$_{20}$) as the structure directing agent (SDA) and under the effects of ethanol. As a polar nonaqueous cosolvent, ethanol has effects on the self-organization behavior of Pluronic P123 in water, which determines the final morphologies of the Li$_2$FeSiO$_4$−C composites synthesized. Li$_2$FeSiO$_4$−C composite nanoparticles are obtained if no ethanol is added into the system during the synthesis process. When tested as lithium-ion battery cathodes, the Li$_2$FeSiO$_4$−C nanoworms show superior electrochemical performances. At the rate of 1 C (1 C = 166 mA g^{-1}) the discharge capacity of the Li$_2$FeSiO$_4$−C nanoworms can reach 166 mAh g^{-1} in the voltage window of 1.5−4.8 V at room temperature. At the rates of 5, 10, and 20 C, the discharge capacities of the Li$_2$FeSiO$_4$−C nanoworms can stabilize at 120, 110, and 90 mAh g^{-1}, respectively, and do not show obvious declines after hundreds of cycles. This performance of the Li$_2$FeSiO$_4$−C nanoworms at high rates is better than that of the Li$_2$FeSiO$_4$−C nanoparticles synthesized and many other Li$_2$FeSiO$_4$/C composites reported in the literature. The excellent electrochemical performances of the Li$_2$FeSiO$_4$−C nanoworms are believed to be related to the small sizes of the Li$_2$FeSiO$_4$ nanocrystals inside the nanoworms and the carbon that coats and embeds the nanocrystals.

KEYWORDS: *Li$_2$FeSiO$_4$−C, nanoworms, cathode materials, lithium ion batteries*
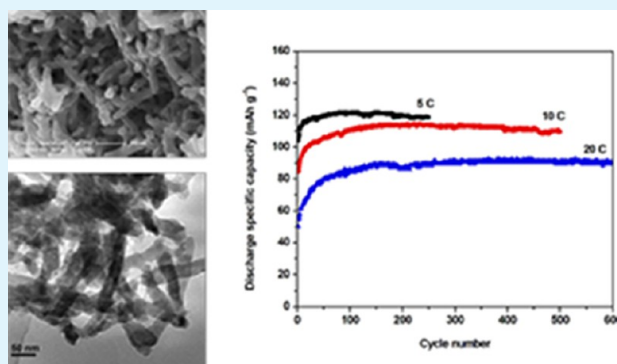
INTRODUCTION

Rechargeable lithium-ion batteries are now in great demand to power portable electronic devices, store electricity from renewable sources, and as a vital component in new electric vehicles (EVs) and hybrid electric vehicles (HEVs).[1−3] Owing to safety and environmental issues, polyanion-type compounds have attracted more and more attention as cathode materials for lithium ion batteries since they were first mentioned in 1997.[4−11] Among the polyanion-type compounds, silicates draw a lot of researchers to devote themselves to this field since two Li$^+$ ions exchange per molecule (redox couple of M^{2+}/M^{4+} for Li$_2$MSiO$_4$) can make the theoretical specific capacity of the material rise to 332 mAh g^{-1}.[12−20] Moreover, Li$_2$FeSiO$_4$ (Li$_2$MSiO$_4$, M = Fe) has advantages like low cost, nontoxicity, high chemical and thermal stabilities, and excellent cycling stability. All these characteristics make Li$_2$FeSiO$_4$ look like a very promising cathode material for next-generation lithium-ion batteries. Although Li$_2$FeSiO$_4$ also suffers from low electronic and ionic conductivities like lithium iron phosphate, approaches like carbon coating and size reduction have been demonstrated to be able to overcome these shortcomings.[21−23]

Morphologies, like sizes, of electrode materials have been shown to have remarkable influences on their electrochemical properties.[24−28] For example, nanoparticle morphology of

electrode materials improves the high-rate performances but causes the volumetric and gravimetric energy density of the electrode to decrease; electrode materials with micro/nano-hierarchical morphologies can ensure excellent high-rate capability and guarantee high tap density at the same time.[29−31] Compared to the much-researched LiFePO$_4$−C composites with various kinds of morphologies, the Li$_2$FeSiO$_4$−C composites synthesized so far have monotonous morphologies. Most Li$_2$FeSiO$_4$−C composites synthesized by the common methods (solid-state reactions, hydrothermal processes, sol−gel methods, et al.) are mainly sphere-like particles or particles without any regular shape. Recently, Rangappa et al. reported that ultrathin nanosheets of Li$_2$FeSiO$_4$ can be synthesized by supercritical fluid method.[32] To the best of our knowledge, this is the only report about Li$_2$FeSiO$_4$−C composites that have special morphologies as the cathode materials for lithium ion batteries so far.

In this paper, nanoworm-like Li$_2$FeSiO$_4$−C composites are synthesized using amphiphilic triblock copolymer P123 as the structure directing agent and under the effects of ethanol.

Amphiphilic triblock copolymers, known as Pluronics, consist of a relatively hydrophobic poly(propylene oxide) (PPO) middle block and two hydrophilic poly(ethylene oxide) (PEO) end blocks. Due to their amphiphilic character, the PEO-PPO-PEO block copolymers exhibit the unique property to self-organize into supramolecular structures in solutions. As a polar nonaqueous selective cosolvent, ethanol has effects on the self-assembly behavior of Pluronic P123 in water, and this effect is used to synthesize Li_2FeSiO_4−C composite with nanoworm-like morphology. When ethanol does not exist in the system, Li_2FeSiO_4−C composite nanoparticles are obtained. When assembled into lithium cells as the cathode materials, the Li_2FeSiO_4−C composite nanoworms show excellent electrochemical performance. At high rates of 5, 10, and 20 C, the discharge specific capacities can stabilize at 120, 110, and 90 mA h g^{-1}, respectively, and do not show any obvious declines for hundreds of cycles.

■ EXPERIMENTAL SECTION

Synthesis of Nanoworm-like Li_2FeSiO_4−C Composites. In a typical synthesis procedure, 2 g Pluronic P123 was dissolved in a mixed solvent of 10 mL ethanol and 30 mL distilled water. An 8 mmol portion of $CH_3COOLi·2H_2O$ and 4 mmol $Fe(NO_3)_3·9H_2O$ were added into the mixed solvent in sequence with magnetic stir until a crimson transparent solution was formed. The solution was then transferred to a cylindrical container for next-step usage. Next, stoichiometric amounts of tetraethyl orthosilicate (TEOS, CP) were dissolved in 40 mL n-hexane, and the n-hexane solution was dropped into the water−ethanol solution in the cylindrical container slowly. After the n-hexane volatilized, the solution was poured into a dish at about 40 °C to evaporate the ethanol and water. When all the solvent evaporated, a thin film was formed. After drying at 100 °C for overnight, the thin film was grounded into powder and calcinated at 650 °C for 10 h in Ar atmosphere. After cooling to room temperature, black Li_2FeSiO_4−C composite powder was obtained.

Characterization. The morphologies of the Li_2FeSiO_4−C composites were investigated using a field-emission scanning electron microscope (SIRION, FEI, USA). Transmission electron microscope (TEM) images were taken on a JEM 2010-FEF (JEOL Ltd., Japan) operating at 200 kV. The crystal structural characterization of the samples was carried out on a Bruker D8 Advance X-ray diffractometer with Cu Kα radiation (λ = 0.15406 nm). The Raman spectra were obtained by using a RM-1000 Renishaw confocal Raman microspectroscope with 514.5 nm laser radiation at a laser power of 0.04 mW in the range of 100−2000 cm^{-1}. The carbon content in the composite was determined by VarioEL III elemental analyzer ((Elementar Analysen System GmbH, Germany). Mössbauer measurements were carried out at room temperature using a Mössbauer spectrometer working with a constant acceleration mode, with ^{57}Co as radiation source and Rh as supporter. The spectra were collected in transmission geometry, and the velocity and isomer shifts were calibrated with α-Fe foil.

Evaluation of Electrochemical Performances. The electrochemical measurements were carried out using CR2016 coin cells with lithium metal disks as the counter electrodes. The working electrodes were made by pressing mixtures of Li_2FeSiO_4−C composite, acetylene black, and polyvinylidene fluoride (PVDF) binder with a weight ratio 75:20:5 on stainless steel meshes which were used as the current collectors. The weight of active materials varied between 3.0 and 4.0 mg cm^{-2} for each cell. The electrolyte was composed with 1 M LiPF$_6$ in ethylene carbonate/dimethyl carbonate (1:1 v/v) solvents and the separator was Celgard 2300 microporous film. The cell was assembled in a glovebox filled with high purity Ar gas. The electrochemical tests were performed galvanostatically at different current densities with voltage window of 1.5−4.8 V on Neware battery test system (Shenzhen, China) at room temperature (20 °C). All the charge−discharge specific capacities were calculated on the net mass of Li_2FeSiO_4 excluding carbon content.

■ RESULTS AND DISCUSSION

The orthosilicate compounds are known to exhibit complex polymorphism, and several structures have been proposed to describe Li_2FeSiO_4. The first was reported by Nytén et al.[12] who suggested an orthorhombic structure, with space group $Pmn2_1$. Later, Nishimura et al.[16] reported the structure of Li_2FeSiO_4 using a monoclinic space group $P2_1$. Most recently, a new crystal structure of γ-polymorph of Li_2FeSiO_4 with space group $Pmnb$ was described by Masquelier et al.[17] The XRD pattern of our as-synthesized composite is shown in Figure 1.
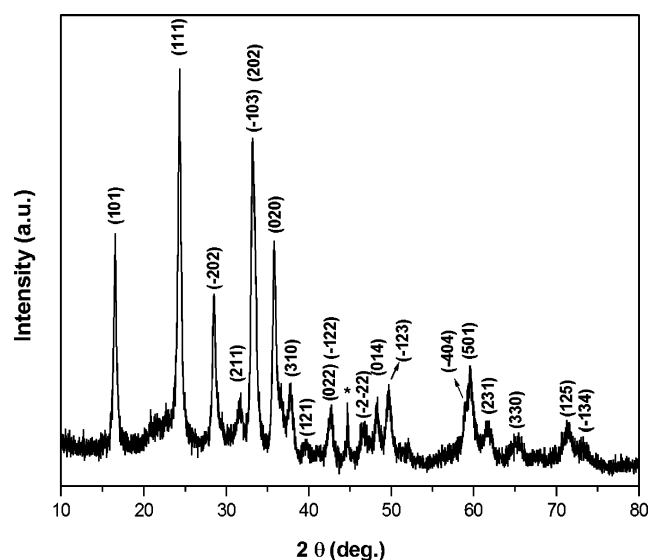
Figure 1. XRD pattern of the as-synthesized Li_2FeSiO_4−C composite.

All the reflection peaks can be indexed on the basis of the monoclinic structured Li_2FeSiO_4 reported by Nishimura et al. (S.G. $P2_1/n$, a = 8.22898 Å, b = 5.02002 Å, c = 8.23335 Å, and β = 99.2027°), suggesting that the as-synthesized composite is single-phase Li_2FeSiO_4.

The morphology of the as-synthesized Li_2FeSiO_4 was identified by field emission scanning electron microscopy (FE-SEM) and high-resolution transmission electron microscopy (HRTEM), and the images are showed in Figure 2. At first glance from the low-magnification SEM image (Figure 2a), it seems that there are a lot of nanoscale "worms" on the sample substrate. The SEM image with high magnification (Figure 2b) shows that the nanoworms are elongated nanoparticles with the ratio of length to diameter at 8:1. From the TEM image (Figure 2c) we can see that these Li_2FeSiO_4 nanoworms have diameters of about 40 nm and lengths of about 300 nm. From the high-resolution TEM image (Figure 2d), it can be noted that there is amorphous carbon not only at the surface, but also inside, of the nanoworms. Li_2FeSiO_4 nanocrystals, with sizes about 5−10 nm, can be found inside the nanoworms. The high-resolution TEM image (Figure 2d, inset, top) and the corresponding Fourier Transform image (Figure 2d, inset, bottom) of a Li_2FeSiO_4 nanocrystal (marked area) inside the nanoworm shows that the distance between two crystal planes is about 0.325 nm, which is very close to the interplanar distance of (−202) planes (0.314 nm) in monoclinic phase of Li_2FeSiO_4.

The Raman spectrum of the as-synthesized Li_2FeSiO_4−C composite nanoworms (Figure 3) shows two bands and can be deconvoluted into four Gaussian bands at 1607, 1541, 1348,

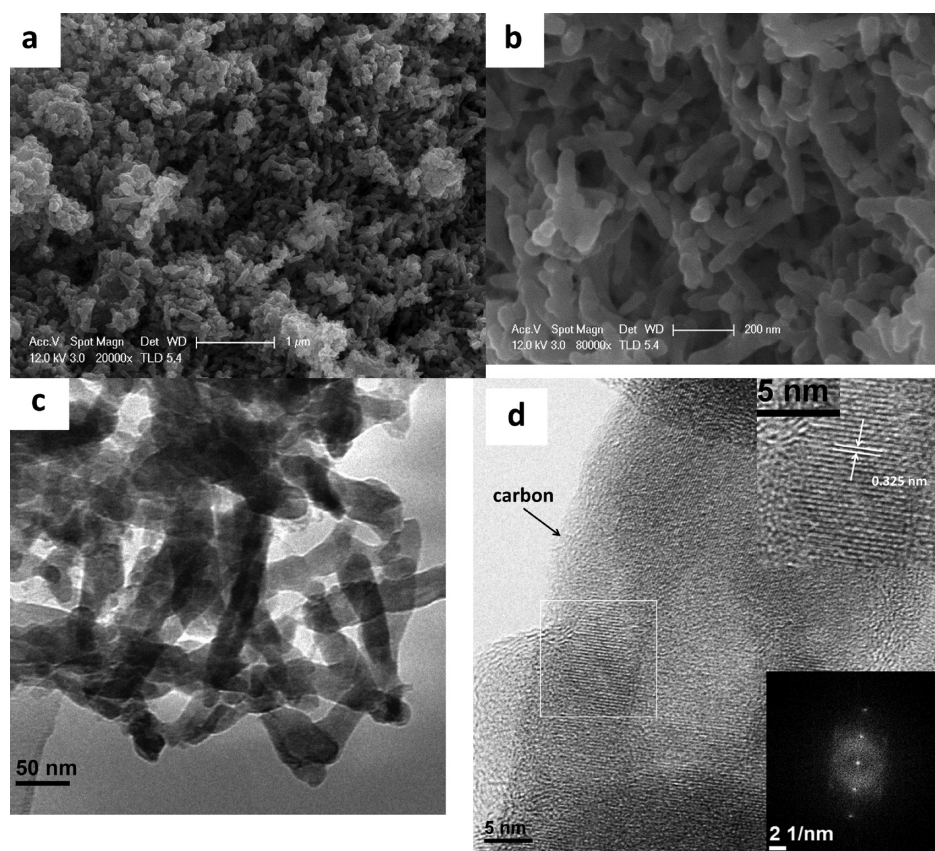**Figure 2.** SEM (a, b), TEM (c), and HRTEM (d) images of the Li$_2$FeSiO$_4$−C composite nanoworms. The insets in figure d are the high-resolution TEM image (top) of a Li$_2$FeSiO$_4$ nanocrystal (marked area) and its corresponding Fourier transform (FT) image (bottom).

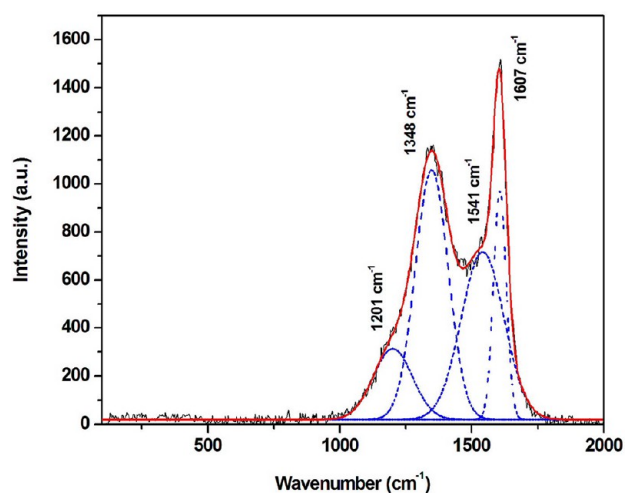**Figure 3.** Raman spectrum of the as-synthesized Li$_2$FeSiO$_4$−C composite nanoworms.

and 1201 cm^{-1}. The peaks at 1348 and 1607 cm^{-1} correspond to the D and G bands of the sp^2-type carbon, respectively, and the peaks at 1201 and 1541 cm^{-1} are related to sp^3-type carbon.[33,34] This spectrum is similar to those previously reported for amorphous carbon materials. Also, no carbon reflection peak can be found in the XRD pattern of the as-synthesized Li$_2$FeSiO$_4$ nanoworms (Figure 1). Thus, the carbon in the composite nanoworms is believed to be amorphous, which leads to the conclusion that the nanoworms are composed of small Li$_2$FeSiO$_4$ nanocrystals that are embedded

in amorphous carbon. By elemental analysis, the mass fraction of carbon in the Li$_2$FeSiO$_4$−C composite is determined to be about 15.45%.

The formation of the Li$_2$FeSiO$_4$−C composite nanoworms is believed to be directed by the self-organization behavior of P123 in selective solvent. In amphiphilic block copolymer−water binary system, the PEO-PPO-PEO block copolymers self-associate forming micelles at relatively low copolymer content and gel phases at higher copolymer contents. They self-assemble into various lyotropic liquid crystalline phases with lamellar, hexagonal, or micellar microstructure.[35] As a consequence of the short E block relative to the length of the P block, P123 (EO$_{20}$PO$_{70}$EO$_{20}$) in dilute solution of water readily associates to form spherical micelles. As a polar nonaqueous cosolvent for water, ethanol makes change to the self-assembly behavior of PEO-PPO-PEO block copolymers.[36] The copolymer P123 in dilute solution self-assembles into spherical micelles in water but forms elongated wormlike micelles in P123-water−ethanol ternary system with proper ethanol concentration.[37] (in our case, the mass concentrations of P123 and ethanol are 5 and 20 wt %, respectively.) The silica oligomers formed by the hydrolysis of the TEOS in the system can be adsorbed readily on the elongated wormlike P123 micelles by hydrogen bonding. In the subsequent aging step (the solution was poured into a dish at about 40 °C to evaporate both the ethanol and water) the elongated wormlike micelles, with silica polymer and charged ions (Li$^+$, Fe^{3+}) adsorbed at the surface, collide, and grow both in the direction of parallel and perpendicular to the long axis of the micelles. Because of the low TEOS concentration (∼2 wt %), the final

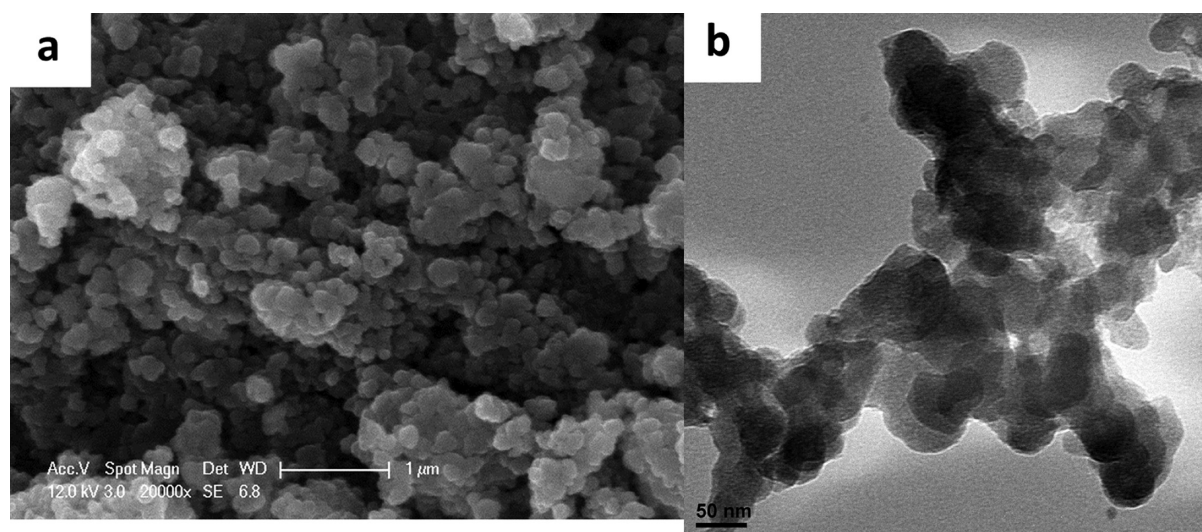**Figure 4.** SEM (a) and TEM (b) images of the as-synthesized Li_2FeSiO_4−C composites nanoparticles when no ethanol is added into the system during the synthesis process.
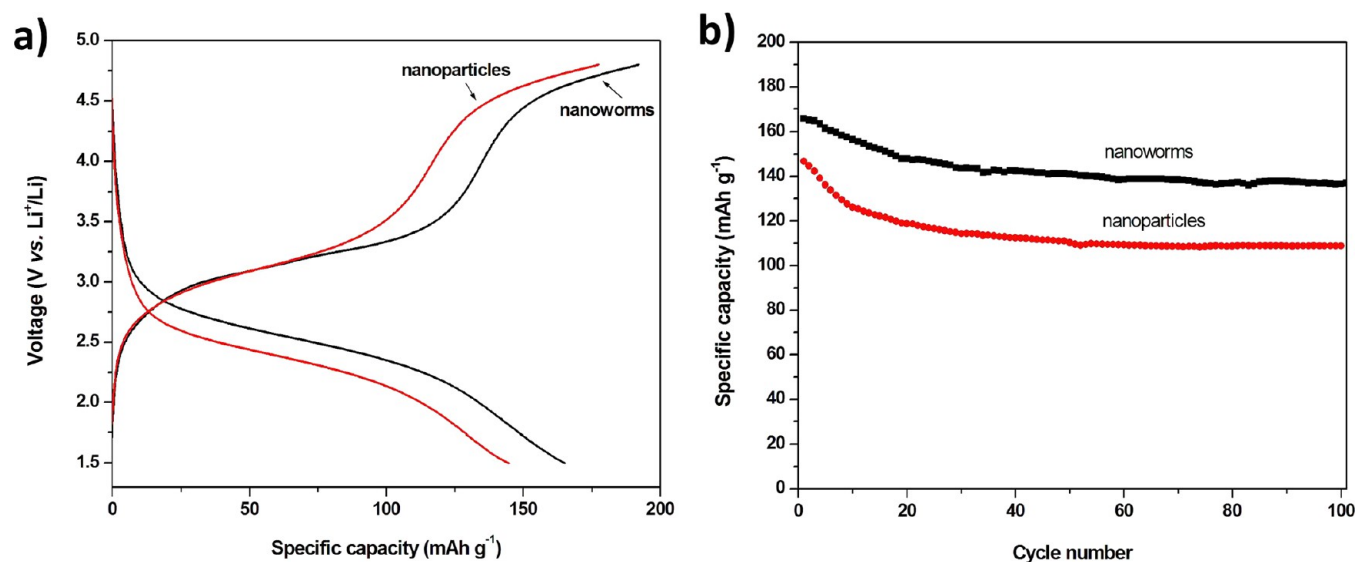

Figure 5. Typical charge−discharge profiles (a) and the cycling behavior (b) of the Li_2FeSiO_4−C composites at the rate of 1 C (1 C = 166 mA h g^{-1}) in the voltage range of 1.5−4.8 V at room temperature.

silica-block copolymer precursors formed have sizes about 40 nm in width and 300 nm in length inheriting the wormlike morphology of the micelles. When the system is calcined in the Ar atmosphere at 650 °C for 10 h, worm-like Li_2FeSiO_4 nanoparticles are formed after the chemical reaction of Li^+, Fe^{3+}, and the silica polymer. During the calcination process, the P123 decomposes and changes into amorphous carbon, which not only acts as reducing agent that reduces the Fe^{3+} ions to Fe^{2+} ions but also embeds the Li_2FeSiO_4 nanocrystals inside the nanoworms.

In order to verify that the ethanol takes effect on the self-assembly behavior of P123 in the system which directs the morphology of the final Li_2FeSiO_4−C composite products, a comparison synthesis experiment was done. In the comparison experiment, the synthesis process and all the experiment parameters were the same as those in the Li_2FeSiO_4−C nanoworms synthesis experiment but without ethanol in the system. The morphology of the Li_2FeSiO_4−C composites thus-

synthesized was shown to be nanoparticles by their SEM (Figure 4a) and TEM images (Figure 4b).

When assembled into rechargeable lithium-ion batteries as the cathode materials, the Li_2FeSiO_4−C composite nanoworms showed excellent electrochemical performances. Galvanostatic charge−discharge measurements were carried out with lithium cells at a current density of 1 C (1 C = 166 mA g^{-1}) to evaluate the electrochemical properties of the Li_2FeSiO_4−C composites. Figure 5a shows the typical charge−discharge curves of both the Li_2FeSiO_4−C composite nanoworms and nanoparticles as cathodes at room temperature in the voltage window of 1.5−4.8 V (vs Li^+/Li). The discharge capacity of the Li_2FeSiO_4−C composite nanoworms in the first cycle can reach 166 mA h g^{-1}, which is the theoretical specific capacity of Li_2FeSiO_4 if only one lithium ion extraction from the Li_2FeSiO_4 molecule is calculated. The discharge capacity of the Li_2FeSiO_4−C composite nanoparticles in the first cycle is 148 mA h g^{-1}, much lower than that of the nanoworms. The cyclability of the Li_2FeSiO_4−C composite nanoworms and nanoparticles as

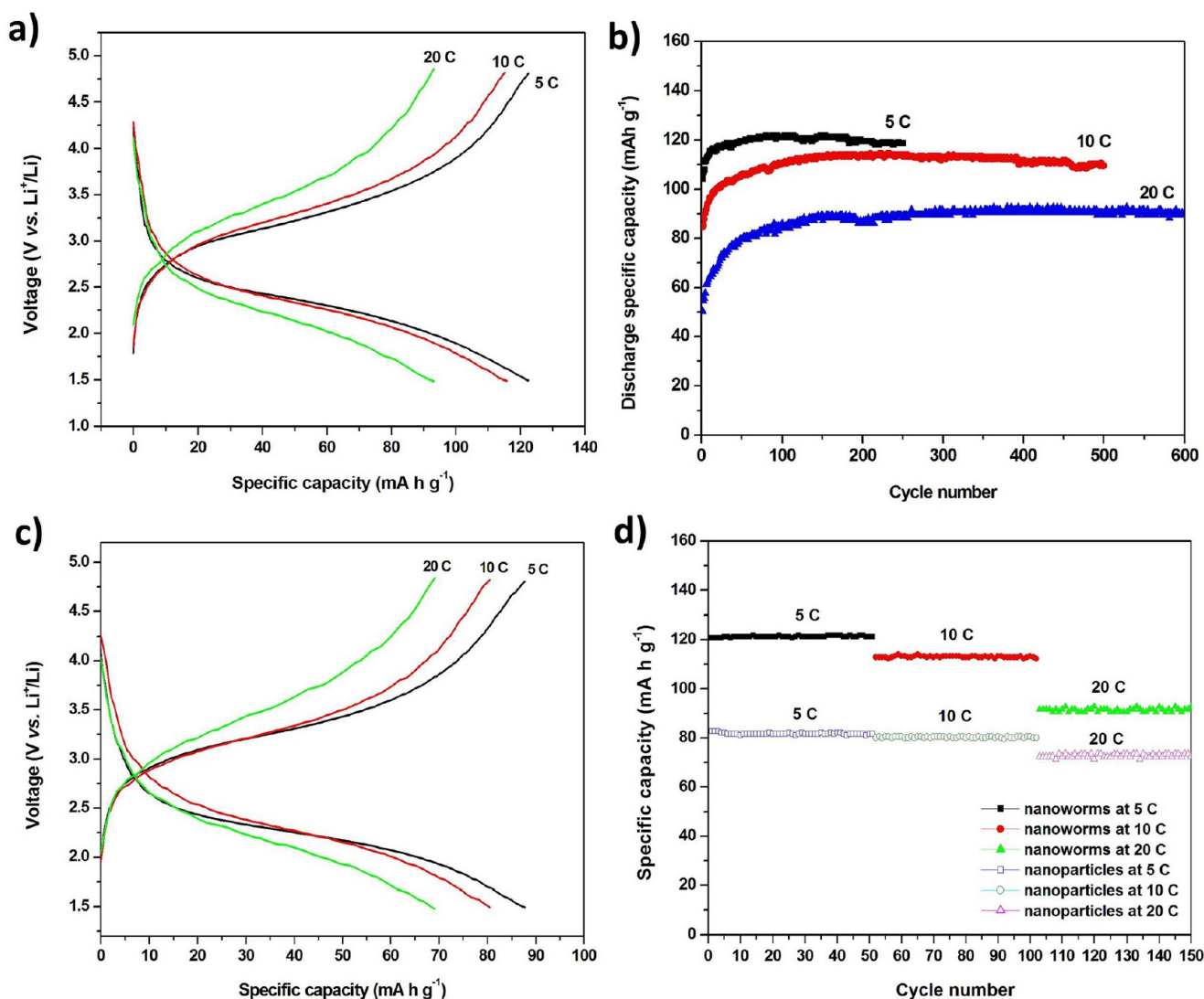**Figure 6.** Typical charge−discharge profiles (a, c) and the cycling behavior (b, d) of the Li_2FeSiO_4−C composites nanoworms and nanoparticles at high rates.

cathodes is shown in Figure 5b. While the discharge specific capacity of the nanoparticles can stabilize at about 110 mA h g^{-1}, the discharge capacity of the nanoworms can stabilize at about 140 mA h g^{-1} at this current density of 1 C (166 mA g^{-1}).

The performance of the Li_2FeSiO_4−C composite nanoworms at high current densities is displayed in Figure 6a and b. Figure 6a shows the typical charge−discharge curves at the rates of 5, 10, and 20 C, respectively, in the voltage window of 1.5−4.8 V (vs Li$^+$/Li) at room temperature (20 °C). Figure 6b shows the cyclability of the Li_2FeSiO_4−C composite nanoworms at different high rates. From this figure we can see that the specific capacities of the cathode increase gradually at the initial stage when the electrode is charge−discharged at high rates. This phenomenon is reasonable when the special nanostructures (Li_2FeSiO_4 nanocrystals embedded in amorphous carbon) of the composite materials are considered. Generally it takes time for the electrolyte in the battery to wet the electrode materials. During this composite-wetting period, the lithium ions in the electrolyte electromigrate through the amorphous carbon in the composite and reach the active materials. In our case, when the electrode is (dis)charged at low

current densities, the lithium ions in the electrolyte have enough time to transport through the amorphous carbon matrix that embeds the Li_2FeSiO_4 nanocrystals in the first charge−discharge cycle. When the electrode is (dis)charged at high rates, however, the time to finish the first cycles is not long enough for the electrolyte to wet the whole composite, and thus, the lithium ions in the electrolyte cannot reach all the Li_2FeSiO_4 nanocrystals in the carbon matrix. (For example, when the electrode is charge−discharged at 1 C, it takes about 60 min to finish the discharging; while it has only about 3 min to finish the discharging when the electrode is charge−discharged at 20 C.) After these initial activation stages, the discharge capacities can reach 120, 110, and 90 mA h g^{-1} at the rates of 5, 10, and 20 C, respectively, and still maintain almost the same capacities after hundreds of cycles. This high-rate performance is excellent compared to the high-rate performances of many other Li_2FeSiO_4−C composites reported in the literature.[18,20,22] For comparison, the high-rate performance of the Li_2FeSiO_4−C composites nanoparticles is also displayed. Figure 6c shows the typical charge−discharge curves for the Li_2FeSiO_4−C composites nanoparticles at the rates of 5, 10, and 20 C, respectively. Figure 6d shows the performances of

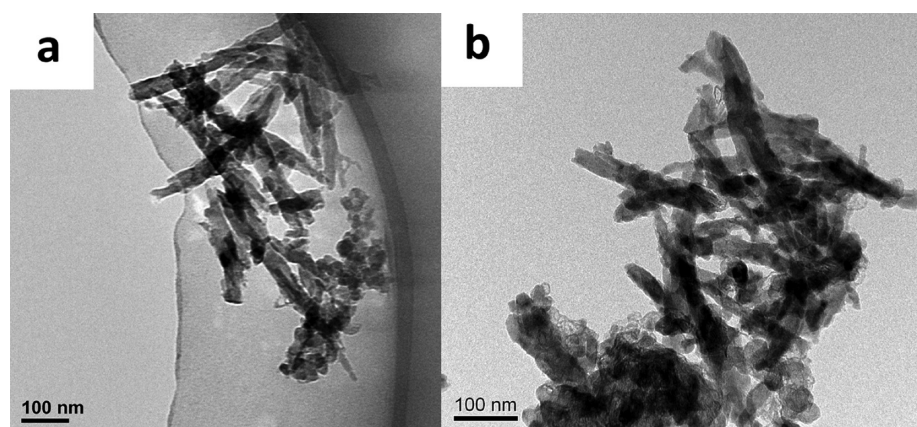**Figure 7.** TEM images of the nanoworm-like Li$_2$FeSiO$_4$−C composite in the cathode before (a) and after (b) cycling at the rate of 10 C (1 C = 166 mA g^{-1}) for 300 cycles.

the nanoworms and nanoparticles at different rates. It shows that the discharge specific capacities of nanoworms are higher than those of nanoparticles for all the high rates.

To see how well the morphology of the electrode materials can maintain, TEM images of the electrode were taken before (Figure 7a) and after (Figure 7b) the electrode was cycled at the rate of 10 C for 300 cycles. Compared to the TEM image of the uncycled electrode, the TEM image of the electrode after cycling for 300 times did not show any distinguishable change in morphology. This high morphology stability may be the root of the high capacity stability of the electrode.

The superior electrochemical performances of these Li$_2$FeSiO$_4$−C composite nanoworms at high rates are believed to be related to their special morphologies. In the Li$_2$FeSiO$_4$−C composite nanoworms, nanocrystals with sizes about 5−10 nm are embedded in amorphous carbon. While the nanocrystals provide short diffusion path length for lithium ions, the amorphous carbon that embeds the nanocrystals increases the electronic conductivity of the materials when used as the cathodes for lithium-ion batteries.

CONCLUSIONS

In summary, Li$_2$FeSiO$_4$−C composite nanoworms have been synthesized using triblock copolymer Pluronic P123 (EO$_{20}$PO$_{70}$EO$_{20}$) as the structure directing agent and under the effect of the polar cosolvent ethanol. Li$_2$FeSiO$_4$−C composites nanoparticles can be obtained when ethanol is not added into the system. The as-prepared Li$_2$FeSiO$_4$−C composite nanoworms are characterized to be nanocrystals with sizes about 5−10 nm embedded in amorphous carbon. The electrochemical properties of these Li$_2$FeSiO$_4$−C composite nanoworms as the cathode materials for lithium ion batteries are measured. The discharge capacity of the material is 166 mA h g^{-1} for the first cycle, and it stabilizes at about 140 mA h g^{-1} at the rate of 1 C in the voltage window of 1.5−4.8 V (vs Li$^+$/ Li) at room temperature. The electrochemical performances of these Li$_2$FeSiO$_4$−C composite nanoworms at high rates are shown to be superior. The discharge capacities can stabilize at 120, 110, and 90 mAh g^{-1} at the rates of 5, 10, and 20 C, respectively, and do not show obvious declines after hundreds of cycles. The small size of the Li$_2$FeSiO$_4$ nanocrystals inside the nanoworms and the carbon network that coats and embeds the nanocrystals are believed to be the main reason for these superior high-rate performances. All these results indicate that Li$_2$FeSiO$_4$−C composite with nanoworm-like morphology is a

very promising candidate as a cheap and sustainable cathode material for the next generation of rechargeable lithium ion batteries.

AUTHOR INFORMATION

Corresponding Author
*E-mail: yxzhang04@whu.edu.cn. Tel.: +86-27-6578-3395. Fax: +86-27-6875-4067.

Notes
The authors declare no competing financial interest.

REFERENCES

(1) Tarascon, J. M.; Armand, M. *Nature* **2001**, *414*, 359.
(2) Armand, M.; Tarascon, J. M. *Nature* **2008**, *451*, 652.
(3) Bruce, P. G.; Scrosati, B.; Tarascon, J. M. *Angew. Chem., Int. Ed.* **2008**, *47*, 2930.
(4) Padhi, A. K.; Nanjundaswamy, K. S.; Goodenough, J. B. *J. Electrochem. Soc.* **1997**, *144*, 1188−1194.
(5) Chung, S. Y.; Bloking, J. T.; Chiang, Y. M. *Nat. Mater.* **2002**, *1*, 123−128.
(6) Herle, P. S.; Ellis, B.; Coombs, N.; Nazar, L. F. *Nat. Mater.* **2004**, *3*, 147−152.
(7) Wang, Y. G.; Wang, Y. R.; Hosono, E.; Wang, K. X.; Zhou, H. S. *Angew. Chem., Int. Ed.* **2008**, *47*, 7461−7465.
(8) Ellis, B. L.; Lee, K. T.; Nazar, L. F. *Chem. Mater.* **2010**, *22*, 691−714.
(9) Goodenough, J. B.; Kim, Y. S. *Chem. Mater.* **2010**, *22*, 587−603.
(10) Yuan, L. X.; Wang, Z. H.; Zhang, W. X; Hu, X. L.; Chen, J. T.; Huang, Y. H.; Goodenough, J. B. *Energy Environ. Sci.* **2011**, *4*, 269.
(11) Gong, Z. L.; Yang, Y. *Energy Environ. Sci.* **2011**, *4*, 3223.
(12) Nytén, A.; Abouimrane, A.; Armand, M.; Gustafsson, T.; Thomas, J. O. *Electrochem. Commun.* **2005**, *7*, 156.
(13) Nyten, A.; Kamali, S.; Haggstrom, L.; Gustafsson, T.; Thomas, J. O. *J. Mater. Chem.* **2006**, *16*, 2266.
(14) Dominko, R.; Bele, M.; Gaberscek, M.; Meden, A.; Remskar, M.; Jamnik, J. *Electrochem. Commun.* **2006**, *8*, 217.
(15) Li, Y. X.; Gong, Z. L.; Yang, Y. *J. Power Sources* **2007**, *174*, 528.
(16) Nishimura, S.; Hayase, I. S.; Kanno, R.; Yashima, M.; Nakayama, N.; Yamada, A. *J. Am. Chem. Soc.* **2008**, *130*, 13212.

2515

dx.doi.org/10.1021/am303047n | ACS Appl. Mater. Interfaces 2013, 5, 2510−2516

(17) Sirisopanaporn, C.; Boulineau, A.; Hanzel, D.; Dominko, R.; Budic, B.; Armstrong, A. R.; Bruce, P. G.; Masquelier, C. *Inorg. Chem.* **2010**, *49*, 7446.

(18) Muraliganth, T.; Stroukoff, K. R.; Manthiram, A. *Chem. Mater.* **2010**, *22*, 5754.

(19) Armstrong, A. R.; Kuganathan, N.; Islam, M. S.; Bruce, P. G. *J. Am. Chem. Soc.* **2011**, *133*, 13031.

(20) Lv, D. P.; Wen, W.; Huang, X. K.; Bai, J. Y.; Mi, J. X.; Wu, S. Q.; Yang, Y. *J. Mater. Chem.* **2011**, *21*, 9506.

(21) Dominko, R. *J. Power Sources* **2008**, *184*, 462.

(22) Gong, Z. L.; Li, Y. X.; He, G. N.; Li, J.; Yang, Y. *Electrochem. Solid-State Lett.* **2008**, *11*, A60.

(23) Zhang, S.; Deng, C.; Yang, S. Y. *Electrochem. Solid-State Lett.* **2009**, *12*, A136.

(24) Chun, L.; Wu, X. Z.; Lou, X. M; Zhang, Y. X. *Electrochim. Acta* **2010**, *55*, 3089.

(25) Saravanan, K.; Reddy, M. V.; Balaya, P.; Gong, H.; Chowdari, B. V. R.; Vittal, J. J. *J. Mater. Chem.* **2009**, *19*, 605−610.

(26) Qian, J. F.; Zhou, M.; Cao, Y. L.; Ai, X. P.; Yang, H. X. *J. Phys. Chem. C* **2010**, *114*, 3477−3482.

(27) Jiao, F.; Bao, J.; Hill, A. H.; Bruce, P. G. *Angew. Chem., Int. Ed.* **2008**, *27*, 9711.

(28) Wang, F.; Yang, J.; Gao, P.; NuLi, Y.; Wang, J. *J. Power Sources* **2011**, *196*, 10258.

(29) Lou, X. M.; Zhang, Y. X. *J. Mater. Chem.* **2011**, *21*, 4156.

(30) Wang, M.; Yang, Y.; Zhang, Y. X. *Nanoscale* **2011**, *3*, 4434.

(31) Sun, C. W.; Rajasekhara, S.; Goodenough, J. B.; Zhou, F. *J. Am. Chem. Soc.* **2011**, *133*, 2132.

(32) Rangappa, D.; Murukanahally, K. D.; Tomai, T.; Unemoto, A.; Honma, I. *Nano Lett.* **2012**, *12*, 1146.

(33) Liu, X. M.; Huang, Z. D.; Oh, S. P.; Ma, C.; Chan, P. C. H.; Vedam, G. K.; Kang, K.; Kim, J. K. *J. Power Sources* **2010**, *195*, 4290.

(34) Doeff, M. M.; Hu, Y. Q.; McLarnon, F.; Kostecki, R. *Electrochem. Solid-State Lett.* **2003**, *6*, A207.

(35) Ivanova, R.; Lindman, B.; Alexandrisdis, P. *Adv. Colloid Interface Sci.* **2001**, *89−90*, 351−382.

(36) Ivanova, R.; Lindman, B.; Alexandridis, P. *Langmuir* **2000**, *16*, 3660−3675.

(37) Chaibundit, C.; Ricardo, N. M. P. S.; Costa, F. M. L. L.; Wong, M. G. P.; Hermida-Merino, D.; Rodriguez-Perez, J.; Hamley, I. W.; Yeates, S. G.; Booth, C. *Langmuir* **2008**, *24*, 12260.